doi:10.1016/j.jmb.2008.09.025 J. Mol. Biol. (2008) 384, 590–603

JMB

Available online at www.sciencedirect.com

ScienceDirect

ELSEVIER

Biochemical and Structural Characterization of an Intramolecular Interaction in FOXO3a and Its Binding with p53

Feng Wang[1,2], Christopher B. Marshall[1,2], Kazuo Yamamoto[2,3,4], Guang-Yao Li[1,2], Michael J. Plevin[1,2], Han You[2,3,4], Tak W. Mak[2,3,4] and Mitsuhiko Ikura[1,2]*

[1]*Division of Signaling Biology, Ontario Cancer Institute, Toronto, Ontario, Canada M5G 2M9*

[2]*Department of Medical Biophysics, University of Toronto, Toronto, Ontario, Canada M5G 1L7*

[3]*The Campbell Family Institute for Breast Cancer Research, University Health Network, 620 University Avenue, Suite 706, Toronto, Ontario, Canada M5G 2C1*

[4]*Department of Immunology, University of Toronto, Toronto, Ontario, Canada M5G 2C1*

Received 9 June 2008; received in revised form 23 August 2008; accepted 2 September 2008
Available online 18 September 2008

Edited by M. F. Summers

FOXO3a, a forkhead transcription factor and member of the forkhead box class O (FOXO) subfamily, has been shown to promote the translocation of p53 to the cytoplasm, thereby inducing the mitochondria-associated apoptotic pathway. However, the binding sites that mediate this interaction between FOXO3a and p53 have not been identified. Here, we show that two regions within FOXO3a, the forkhead (FH) DNA binding domain and a conserved C-terminal transactivation domain (CR3), interact with the DNA binding domain of p53, with affinities in the low millimolar range and low micromolar range, respectively. Our data further suggest that within the FOXO3a molecule, the FH and CR3 domains engage in an intramolecular interaction with low micromolar affinity. Moreover, we used NMR to determine the solution structure of the FH domain. This enabled us to map the binding site for the CR3, which overlaps with the DNA binding site. We demonstrate that an intrinsically disordered linker between the FH and CR3 domains is required for full p53 binding activity. We also show that p53 disrupts the intramolecular interaction between FH and CR3. These results provide evidence for interplay of the FH and CR3 domains in association with p53.

Keywords: FOXO3a; p53; intramolecular interaction; NMR; apoptosis

**Corresponding author.* Division of Signaling Biology, Ontario Cancer Institute, Toronto, Ontario, Canada M5G 2M9. E-mail address: mikura@uhnres.utoronto.ca.

Present addresses: M. J. Plevin, Laboratoire de RMN, Institut de Biologie Structurale 41, rue Jules Horowitz, Grenoble 38027, France; H. You, Key Laboratory for Cell Biology and Tumor Cell Engineering of the Ministry of Education, School of Life Sciences, Xiamen University, Fujian 361005, China.

Abbreviations used: FH, forkhead; FOX, forkhead box; FOXO, forkhead box class O; DBD, DNA binding domain; HSQC, heteronuclear single quantum coherence; CSI, chemical shift index; NOE, nuclear Overhauser enhancement; NOESY, nuclear Overhauser enhancement spectroscopy; TA, transactivation; TET, tetramerization; NES, nuclear export signal.

Introduction

The forkhead box (FOX) protein family is composed of more than 100 transcription factors that have been divided into 19 subfamilies (FOXA to FOXS).[1] The FOX class O (FOXO) subfamily contains 4 mammalian members: FOXO1 (FKHR), FOXO3a (FKHRL1), FOXO4 (AFX), and FOXO6.[2] The FOXO subfamily has been the subject of much interest, differing from the other subfamilies by the presence of a 5-aa insertion within the forkhead (FH) DNA-binding domain.[3] FOXO3a, the most studied member of the FOXO transcription factors, is expressed in most human tissues[4] and is involved in metabolism, cell cycle arrest, cell differentiation, and apoptosis.[5–11]

FOXO3a has recently been found to activate apoptotic pathways via two distinct functions. First, FOXO3a activates the transcription of many genes, including $p27^{Kip1}$ and the androgen receptor, which induce cell growth arrest, as well as the apoptotic proteins Bim and PUMA. By doing so, it plays a role in the balance between cell survival and cell death.[5–11] Second, FOXO3a promotes the direct mitochondrial functions of p53 as an apoptotic regulator.[12] Upon activation by serum starvation, FOXO3a binds directly to p53, which can be detected *in vivo* by immunoprecipitation. Moreover, this interaction decreases the DNA binding activity of p53 and promotes cytoplasmic translocation of p53.[13] In response to apoptotic stimuli, cytoplasmic p53 is directed to the mitochondrial outer membrane, where it interacts with, and suppresses, the antiapoptotic function of Bcl-2 and Bcl-xL, the repressors of pro-apoptotic Bak/Bax.[14] As the expression of PUMA increases, induced in part by FOXO3a,[11] PUMA displaces p53 from Bcl-xL/Bcl-2. In turn, p53 promotes the oligomerization of Bax, leading to the liberation of cytochrome *c* from the intermembrane space of the mitochondria into the cytoplasm,[15–17] thus activating the caspase cascade and resulting programmed cell death.[18,19] Although the interaction between FOXO3a and p53 is observed with both full-length and FH deletion mutant of FOXO3a, the FH domain is required to stabilize p53 from degradation, disrupt the DNA binding activity of p53, and induce apoptosis.[13]

Despite increasing interest in the biological significance of FOXO3a in apoptosis, structural information is largely elusive. FOXO3a is a 71-kDa protein containing a winged-helix FH domain that is conserved among all FOX proteins. This particular protein also confers sequence-specific DNA binding to the FH response element.[20] The DNA binding site is composed of helix 3 (H3), a long unstructured loop wing 1 (W1), the C-terminal wing 2 (W2), and the N-terminus of the FH domain (Fig. 1a and b).[10,21,22] FOXO3a also contains three additional conserved regions designated as CR1–CR3 (Fig. 1a). The CR3 domain is an acidic region found at the C-terminus and has been shown to function as a transactivation domain that is required for coactivator recruitment (Fig. 1c).[23,24] However, the binding site for p53 has not been characterized. Here, we demonstrate that both FH and CR3 domains directly bind p53. Our *in vitro* biochemical studies also show that these two domains engage in an intramolecular interaction. The present NMR characterization of FOXO3a sheds some light on the structural basis of FOXO3a–p53 interaction and on the intramolecular association between the FH and CR3 domains.

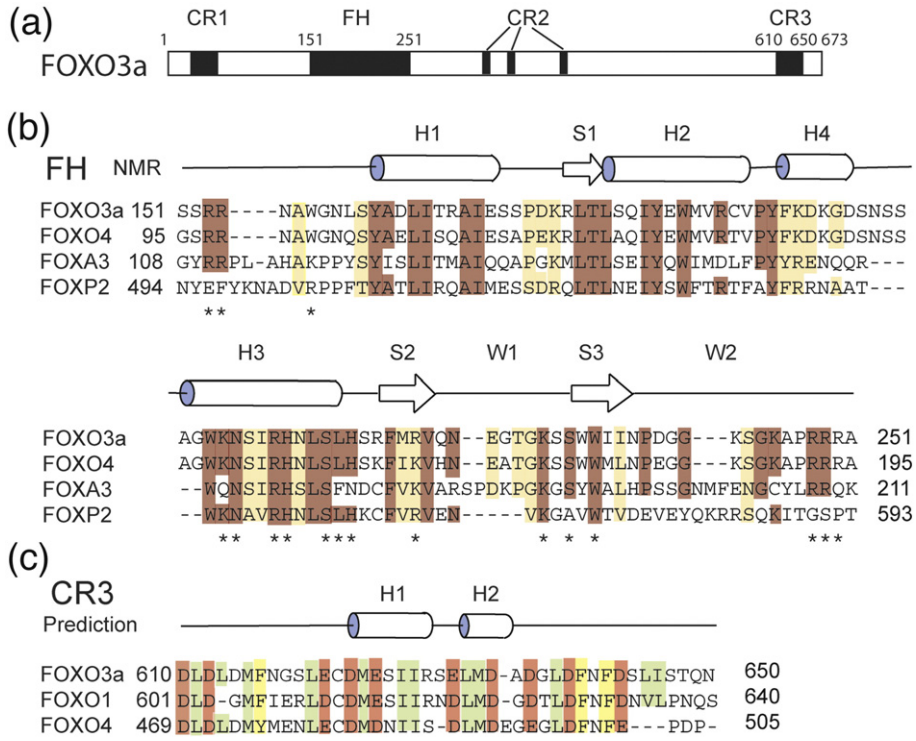

Fig. 1. Domain structure of FOXO3a and sequence alignments. (a) The domain architecture of FOXO3a is shown with the well-folded FH domain, and three other conserved regions, CR1–CR3, are indicated. (b) The sequence alignment of the FH domains of different FOX proteins with the secondary structure derived from the solution structure of the FH domain of FOXO3a (cylinders, α-helices; arrows, β-strands; lines, loops) is shown. Identical residues are shown in dark brown, and residues of a similar type are shown in light brown. The star marks underneath indicate residues that interact with DNA based on known FH–DNA complex structures or previous biophysical studies. (c) The sequence alignment of the CR3 domains of FOXO proteins is shown at the bottom with the predicted secondary structure (PSIPRED). Conserved residues are shown in different colors according to residue type (orange, negatively charged residue; green, nonpolar residue; yellow, aromatic residue). The residue numbers of all domains are listed.

Results

FOXO3a–p53 interaction

To map the p53 binding site(s) on FOXO3a, we conducted pull-down assays with full-length glutathione *S*-transferase (GST)–p53, and several different Myc-tagged FOXO3a truncation and deletion mutants, expressed in an *in vitro* transcription/translation system (Fig. 2a). The results indicate that the N-terminus of FOXO3a (M1–C150) is not required for p53 binding. However, further truncation of the structured part of the FH domain (S151–S243) reduces binding affinity to some extent. We also determined that the C-terminus of FOXO3a is

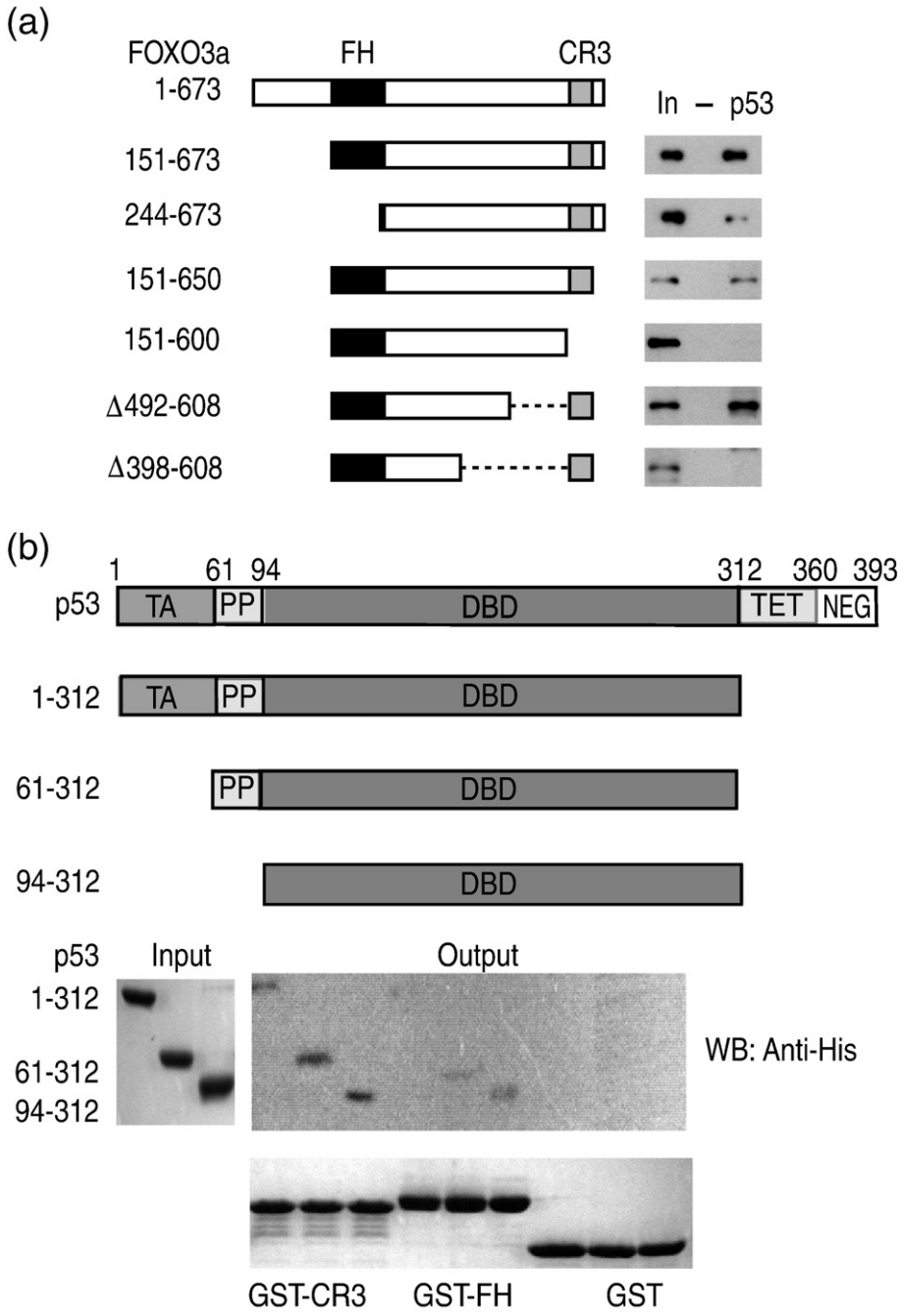

Fig. 2. GST pull-down assays of the FOXO3a–p53 interaction. (a) Full-length GST–p53 was used to pull down different *in vitro*-translated Myc-FOXO3a truncation or deletion mutants. The amino acid numbers of each mutant are labeled on the left. Relative affinities were estimated by comparing the ratio of the intensity of bands from output and input. The negative control with GST alone is also shown in the middle lane. (b) The domain architecture of p53 is shown on top: TA domain, polyproline domain, DBD, TET domain, and negative-regulation (NEG) domain. Three His-tagged p53 constructs were used to define the FOXO3a binding site. The left and bottom panels of the input and the loading control were visualized by Coomassie blue stain, while the output was detected by Western blotting.

crucial for p53 binding as C-terminal truncation (V601–N650) reduced affinity. Finally, the linker region between the FH and CR3 domains also contributes to the interaction with p53. The deletion of residues L492–P608 does not affect p53 binding, whereas a longer deletion of residues P398–P608 reduces the binding, despite the fact that the construct contains both FH and CR3 domains. These results suggest that interaction with p53 is not conferred by a single motif of FOXO3a but that several parts of FOXO3a are in fact involved in p53 binding.

To define the FOXO3a binding site within p53, we further performed GST pull-down assays using bacterially expressed and purified FOXO3a and p53 constructs. p53 is a tumor suppressor with 393 residues, including an N-terminal transactivation (TA) domain, a polypropline (PP) domain, a DNA-binding domain (DBD), a tetramerization (TET) domain, and a C-terminal negative regulatory domain (Fig. 2b).[25] Three His-tagged p53 constructs, $p53_{1–312}$, $p53_{61–312}$, and $p53_{94–312}$, were generated to test their binding to GST-tagged FOXO3a FH (S151–A251) and CR3 (D610–N650) domains, which we refer to as GST-FH and GST-CR3, respectively. The $p53_{94–312}$ and $p53_{61–312}$ constructs bind to GST-CR3 with similar affinities; however, $p53_{1–312}$ appears to bind less strongly, suggesting that the TA domain (M1–P60) interferes with binding of CR3. The p53 TA domain and the FH–CR3 domain are both very acidic; thus, we speculate that they may compete for interaction with the basic DBD or that repulsive charge interactions might decrease binding between CR3 and p53. Similarly, $p53_{61–312}$ and $p53_{94–312}$ also display higher affinity compared with $p53_{1–312}$ for GST-FH (Fig. 2b). These results indicate that the FOXO3a binding sites on p53 are found within residues S94–T312, which contain the DBD of p53. Additionally, the results show that all three p53 constructs bind to GST-CR3 with greater affinity than they do to GST-FH.

Solution structure of FH domain

In order to gain further insight into the structural basis for FOXO3a–p53 interaction, we determined the solution structure of the FH domain (residues S151–A251) of FOXO3a. First, we checked the biological activity of the purified recombinant FH domain; we determined that it was capable of binding 18- and 12-bp DNA duplex constructs derived from the PUMA promoter, as evidenced by electrophoretic mobility shift assay and NMR experiments, respectively (Supplemental Fig. 1). We performed standard triple-resonance NMR experiments,[26] which yielded nearly complete backbone assignments (Fig. 3a) as well as >90% side-chain assignments. The chemical shift index (CSI) (Fig. 3b)[27] as well as ^{15}N- and ^{13}C-edited nuclear Overhauser enhancement spectroscopy (NOESY) analysis (Supplemental Fig. 2a) were used to calculate a solution structure of the FOXO3a FH domain (Fig. 3c; Supplemental Fig. 2b and Table 1). The solution structure of the FH domain of FOXO3a adopts the winged-helix fold as expected, exhibiting three stacking major α-helices (H1–H3) and two large unstructured wings (W1, W2). It also contains a small helix (H4) between H2 and H3 and three β-strands (S1–S3), which form an antiparallel β-sheet (Fig. 3c). The FH domain of FOXO3a is composed of the same fold as FOXO4 (Supplemental Fig. 2c) [Protein Data Bank (PDB) code 1E17],[28] which is not surprising considering the high level of similarity in sequence (about 80% identity).

The CSI values of residues 178–180 are negative, indicating that these residues form a short β-strand (S1) (Fig. 3b). An NOE signal is visible between L178NH and W234NH, which are found in S1 and S3, respectively, indicating pairing between these two strands (Supplemental Fig. 2a). Nevertheless, the first small β-strand S1 is not well defined in the solution structure. The small helix H4 is ill-defined in the present structure of the FH domain of FOXO3a with flexible boundaries in different conformers, and uncertainty as to whether H4 is an α-helix or a 3_{10}-helix remains, consistent with the reported solution structure of the FOXO4 FH domain.[28] For both FOXO3a and FOXO4, the H4 is preceding or partially overlapped with a 5-residue insertion (198–GDSNS–202 in FOXO3a), which is absent in other FOX subfamilies.[3] In the recently reported crystal structure of the FOXO3a FH–DNA complex (PDB code 2uzk), this helix is disordered and solvent exposed.[21] In our 20-conformer ensemble, H4 and H3, which binds the major groove of DNA,[21] form ordered secondary structures but lack coordinate precision compared with H1 and H2 (Supplemental Fig. 2b). The same situation was also observed in the FOXO4 FH solution structure, for which steady-state NOE measurements suggest that this region is dynamic and flexible.[28] The intrinsic flexibility of the DNA binding site may be important for target sequence searching and binding of DNA.

Intramolecular interaction between FH and CR3

Similar to many eukaryotic transcription factors that possess intrinsically disordered regions,[29] FOXO3a is predicted to be largely unstructured. We performed secondary structure and disorder prediction analysis using PSIPRED,[30] and the results strongly suggest that the region (V252–S609) between the FH domain and the CR3 domain is largely disordered and unstructured, whereas both FH and CR3 domains are folded. In the light of the GST pull-down data showing that both FH and CR3 domains are involved in interaction with p53 (Fig. 2a and b), we speculated that these domains may be situated in close proximity within the FOXO3a molecule, even though they are separated by ~350 unstructured amino acids in the sequence. Moreover, the FH domain is positively charged ($pI=10.52$) and the CR3 domain is negatively charged ($pI=3.37$), suggesting the possibility of electrostatic interaction. In order to examine this potential intramolecular interaction, we conducted a GST pull-down assay with bacterially expressed and purified GST-FH (S151–A251) and His-Trx-CR3 (D610–N650). The results

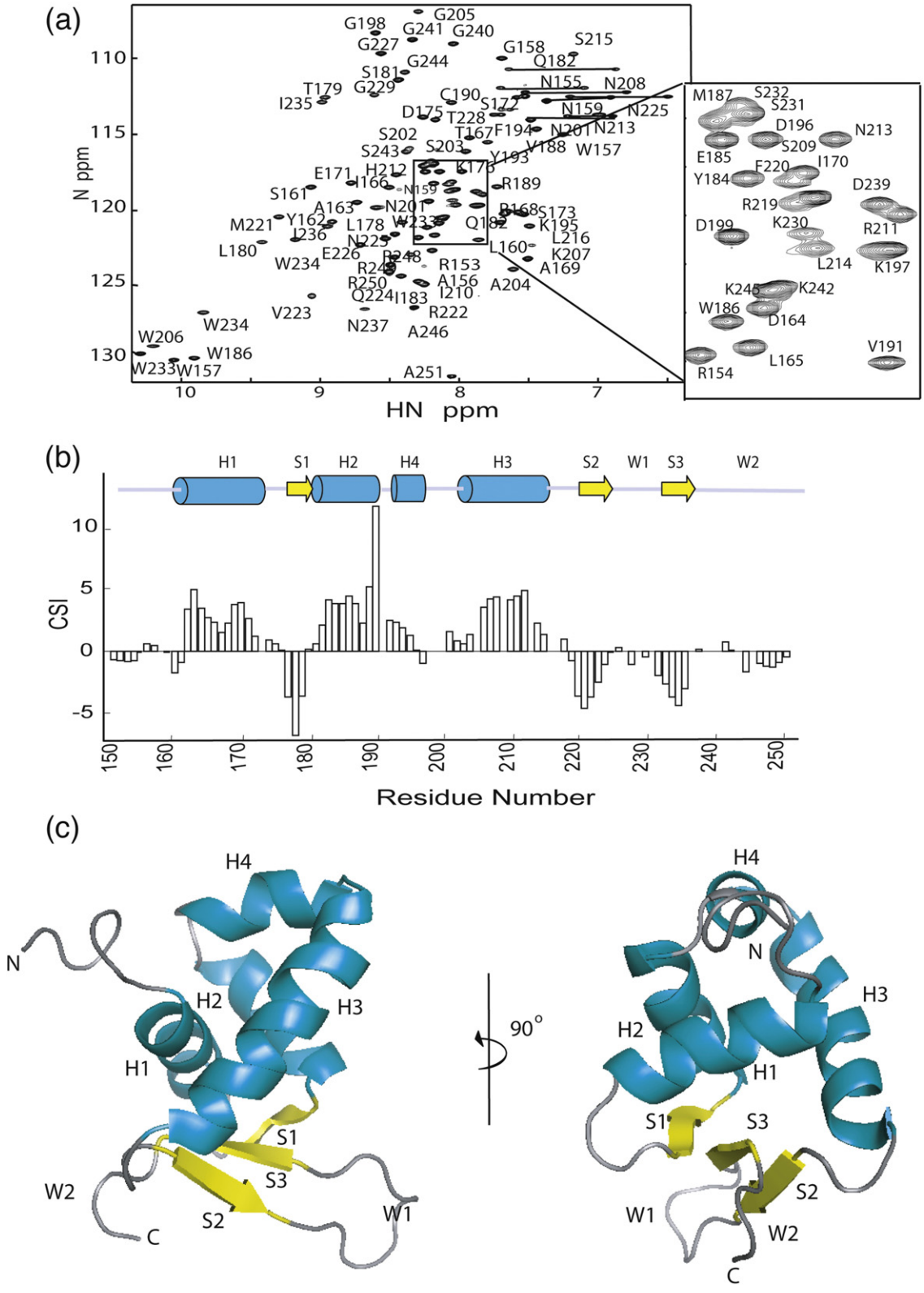

Fig. 3. NMR spectroscopy and solution structure of the FH domain of FOXO3a. (a) The cross-peaks of ^{1}H–^{15}N HSQC spectrum of the FH domain of FOXO3a are assigned, and the assignments of 93 (of 97 nonproline residues) backbone signals as well as side-chain signals are labeled. Cross-peaks corresponding to the same side chain are connected with horizontal lines. (b) CSI *versus* residue number are shown, with consecutive positive CSI values indicating α-helix (cyan cylinders) and consecutive negative values indicating β-strand (yellow arrows). Four helices and three strands are defined as H1–H4 and S1–S3, respectively, consistent with the nomenclature used to describe homologue FH domains. (c) Ribbon model of the FH domain of FOXO3a (R154–G240). The structure is shown from two angles, and N- and C-termini and secondary structure components are labeled (cyan, helix; yellow, strand; gray, loop).

clearly show that His-Trx-CR3 binds to GST-FH but not to GST alone and that His-Trx alone does not bind to GST-FH (Supplemental Fig. 3a).

We then employed NMR spectroscopy to obtain structural insights into this FH–CR3 interaction. The ^{15}N-labeled FH domain was titrated with unlabeled CR3 peptide, and a series of ^{1}H–^{15}N heteronuclear single quantum coherence (HSQC) spectra were recorded with increasing concentrations of CR3 (Fig. 4a). A number of peaks shifted from the free-state positions to the CR3-bound-state positions in a "fast-exchange" fashion on the NMR timescale, suggesting that the interaction is of moderate affinity. Mapping the chemical shift perturbation on the FH

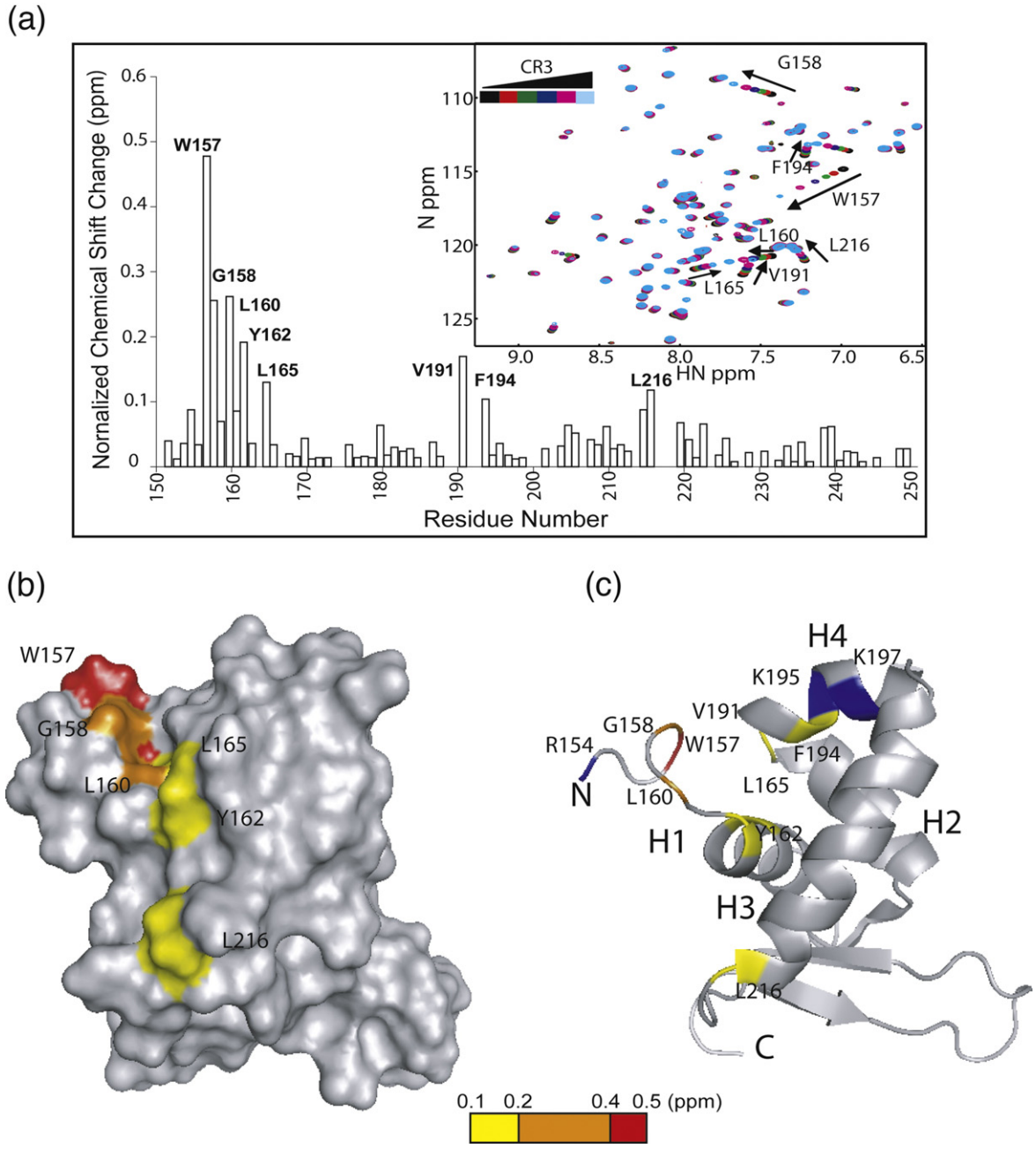

Fig. 4. NMR titration and binding site mapping of CR3 on FH. (a) ^{1}H–^{15}N HSQC spectra show ^{15}N-labeled FH domain titrated with unlabeled CR3 peptide (right corner). With increasing CR3 concentration, the spectra shifted from black to red, green, blue, pink, and cyan. The normalized backbone amide ^{15}N,^{1}H chemical shift change was calculated using the equation $\Delta CS = \sqrt{(\Delta H)^2 + (\Delta N/6.5)^2}$ and plotted *versus* residue number. Residues with large normalized chemical shift change (>0.1 ppm) are labeled. (b) An annotated molecular surface representation of the FH domain of FOXO3a shows the location of residues undergoing large chemical shift perturbation upon CR3 titration, revealing the CR3 binding site on the FH domain. The scale indicates the magnitude of the normalized chemical shift change. V191 and F194 are buried and therefore not visible on the surface. (c) The same residues are labeled in the ribbon diagram of the FH domain together with the positively charged residues in the vicinity of the binding site (blue), indicating that N-terminus, H1, H2, H4, and H3 comprise the binding surface.

structure (Fig. 4b) revealed the binding surface for CR3 peptide. Three aromatic residues (W157, Y162, and F194) at the N-terminus and H4 of the FH domain are most affected. Three leucine residues (L160, L165, and L216) and one valine (V191) are also affected (Fig. 4a). Together, these residues form a hydrophobic crevice. These results strongly suggest that the CR3 region of FOXO3a binds the FH in the hydrophobic crevice, formed by the N-terminal loop, H1, H4, and H3 (Fig. 4c). It is important to note that in the vicinity of this hydrophobic cleft are four positively charged residues, R153, R154, K195, and K197 (Fig. 4c), which would be candidates for interaction with acidic residues of the CR3 (i.e., D623, E625, E631, D634, and D636). Interestingly, this CR3 binding site overlaps with the DNA binding sites that are composed of H3, H4, W1, W2, and the N-terminal loop.[21,22]

p53 competes with FH for a binding site in CR3

Our pull-down assays have shown that the CR3 domain interacts directly with the DBD of p53, and our NMR titration also demonstrated that the CR3 domain interacts with the FH domain of FOXO3a.

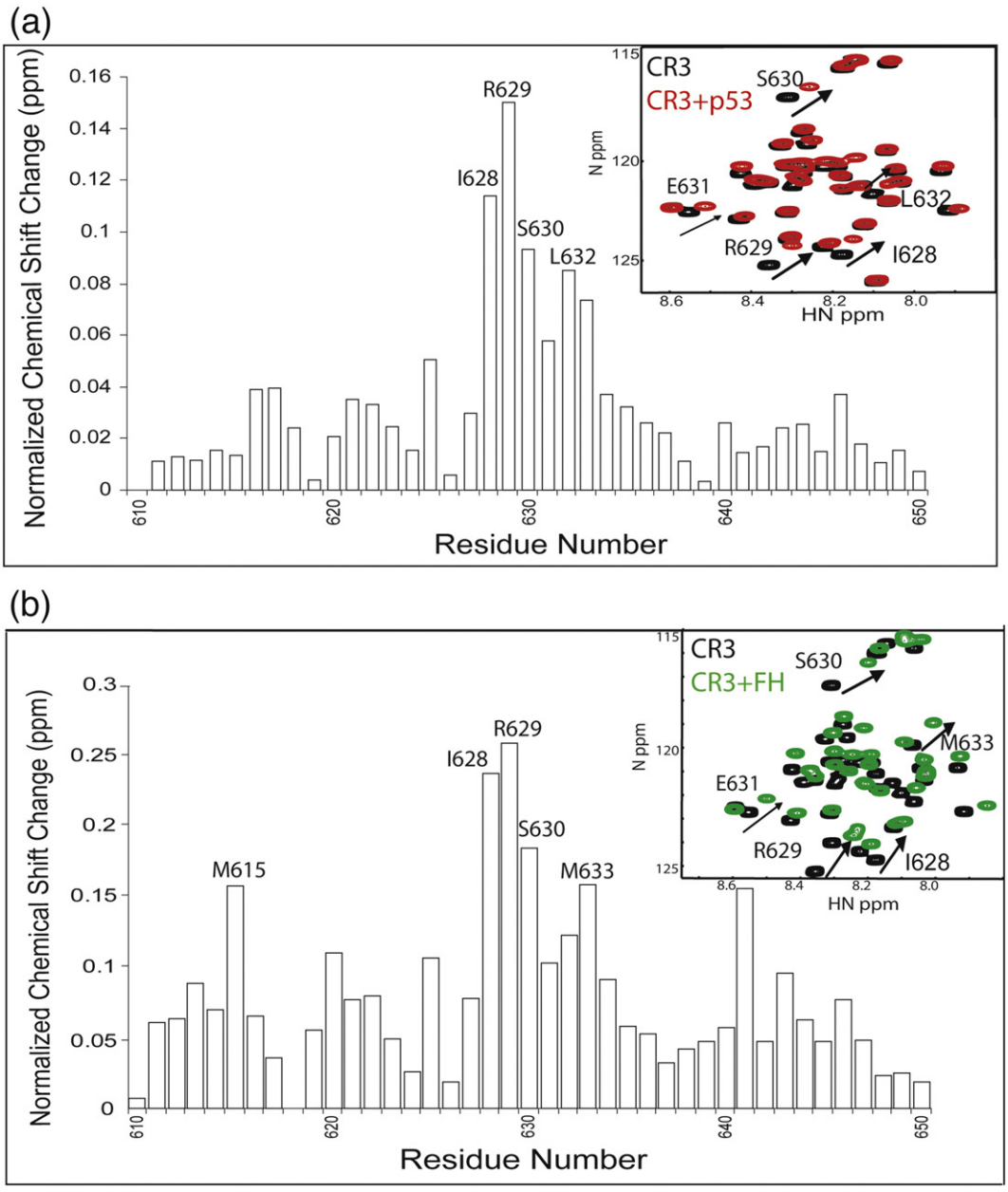

Fig. 5. Chemical shift perturbation of the CR3 domain upon p53 and the FH domain binding. (a) The two overlaid ^{1}H–^{15}N HSQC spectra (black, CR3; red, CR3+p53) show the chemical shift perturbation of ^{15}N-labeled CR3 domain upon addition of (1:2) $p53_{61–312}$ (right), and the normalized chemical shift changes are plotted *versus* residue number. The residues with the largest chemical shift changes accumulate in the middle core region of the CR3 domain (E625–M633). (b) The ^{1}H–^{15}N HSQC spectra (black, CR3; green, CR3+FH) show the ^{15}N-labeled CR3 domain upon FH binding (right) with a ratio of 1:2, and the normalized chemical shift changes were plotted *versus* residue number. The same core region of the CR3 domain (I627–A635) and M615 exhibit more severely perturbation compared with other parts.

Thus, we investigated whether p53 and FH bind to the same region within CR3. We purified ^{15}N-labeled CR3 (D610–N650) and recorded ^{1}H–^{15}N HSQC spectra of the CR3 domain with and without unlabeled $p53_{61–312}$ (Fig. 5a). We determined which residues are involved in p53 interaction based on chemical shift perturbation induced by a two-fold excess of p53 and found that a central portion of CR3 consisting of E625 to M633 is most perturbed (Fig. 5a). This core region is composed of several nonpolar residues (I627, I628, L632, and M633), which are conserved in this protein subfamily, as well as negatively charged residues (E625, D623, E631, and D634). This central core region is predicted by PSIPRED to be helical (Fig. 1c); however, the lack of chemical shift dispersion in the ^{1}H–^{15}N HSQC spectrum and that in the CD spectrum of the free CR3 peptide suggest that this region is mainly unstructured when isolated in solution.

Similar NMR titration experiments were performed with unlabeled FH to map the residues of the CR3 involved in the FH–CR3 interaction. The subset of CR3 peaks that were perturbed by addition of FH was largely the same as that affected by $p53_{61–312}$ titration (Fig. 5b), suggesting that the FH domain and p53 bind to the same ~9-residue core region of CR3. Because the CR3 binding site on the FH domain is a hydrophobic crevice surrounded by positively charged residues and the CR3 is composed of conserved, nonpolar, and negatively charged residues, the FH–CR3 interaction is likely mediated by both hydrophobic and electrostatic interactions.

The p53 DBD and the FOXO3a FH domain interact with the same core region of the CR3 domain, raising the question of whether these interactions are mutually exclusive. To compare the binding affinities of CR3 with the FH domain and p53, we performed NMR titration experiments with ^{15}N-labeled CR3 and unlabeled FH and $p53_{61–312}$. Comparing the titration curves of CR3 residue R629, we obtained similar apparent K_d values for the CR3–FH and CR3–p53 interactions, which are 19±12 and 14±12 μM, respectively (Fig. 6a). We also used the ^{1}H–^{15}N HSQC spectra of ^{15}N-labeled FH as a probe to detect direct competition between the FH domain and p53 in interacting with the CR3 domain (Fig. 6a). The addition of $p53_{61–312}$ induced only very small changes in the FH domain spectrum (Fig. 6a, middle column). In contrast, the addition of CR3 peptide induced marked changes in many peaks in the spectrum (from black to red; Fig. 6a, right column). We then added unlabeled $p53_{61–312}$ into the mixture of ^{15}N-labeled FH domain and unlabeled CR3 peptide. With increasing $p53_{61–312}$ concentration, peaks that were perturbed upon CR3 addition (e.g., W157 and G158) moved back toward their original free-state positions (Fig. 6a, right column). These results indicate that $p53_{61–312}$ competes with the FH domain for CR3 peptide and disrupts the FH–CR3 interaction to a certain extent. Moreover, the FH spectrum was broadened by $p53_{61–312}$ (Fig. 6a), likely due to the exchange between free FH domain and CR3-bound FH domain and possible interaction between FH and p53.

Linking the FH and CR3 domains increases affinity for p53

In order to gain more insight into FOXO3a–p53 interaction, we attempted to express and purify full-length FOXO3a, as well as an N-terminal truncated construct encoding S151–G673. However, these constructs, which contain a predicted long flexible linker between the FH and CR3 domains, could not be expressed and purified due to their susceptibility to proteolysis. In order to mimic the long unstructured flexible linker predicted in full-length FOXO3a, we decided to fuse the FH and CR3 domains via a $(Gly–Ser)_4$ linker. We found that, although it is of low quality, the spectrum of ^{15}N-labeled FH–CR3 fusion protein is similar to that of the ^{15}N-labeled FH domain in the presence of CR3 peptide (Fig. 6b; Supplemental Fig. 3b), demonstrating that the interaction between the FH domain and the CR3 domain is maintained in the fusion construct. Thus, the FH–CR3 fusion protein could serve as a reasonable model for the full-length FOXO3a molecule.

We performed GST pull-down assays to compare the affinity of GST-CR3 and that of GST-FH–CR3 fusion protein for p53. We used increasing concentrations of the His-tagged p53 DBD, $p53_{94–312}$, as the input and found that this construct binds to the GST-FH–CR3 fusion protein more strongly than it does to GST-CR3 (Fig. 6c). This suggests that the FH domain and CR3 domain simultaneously bind to p53, thereby enhancing the binding affinity for p53.

Discussion

The tumor suppressor p53 is central to both cell cycle control and apoptosis and is also one of the most frequently mutated genes in human cancers.[31,32] As such, p53 protein is involved in many signaling networks.[33] A recent study by You *et al.* revealed a new link between p53 and FOXO3a in apoptosis that involves FOXO3a-mediated recruitment of p53 to the cytoplasm, where it promotes apoptosis by inhibiting the antiapoptotic proteins Bcl-xL and Bcl-2 in the mitochondrial outer membrane.[13] This translocation of p53 from the nucleus to the cytoplasm was shown to involve a conformational change in p53, and FOXO3a has been implicated in the translocation.[13] The present study attempted to address many questions surrounding the FOXO3a-mediated p53 activation in its cytoplasmic function. We have demonstrated that FOXO3a interacts directly with the DBD of p53 and that both FH and CR3 domains of FOXO3a play crucial roles in the p53 interaction (Fig. 7). In addition, those functional domains of FOXO3a participate in an internal interaction facilitated by the long connecting domain linker (V252–S609), which was predicted to be disordered (Fig. 7).

The functions of many transcription factors are mediated by intrinsically disordered regions, which

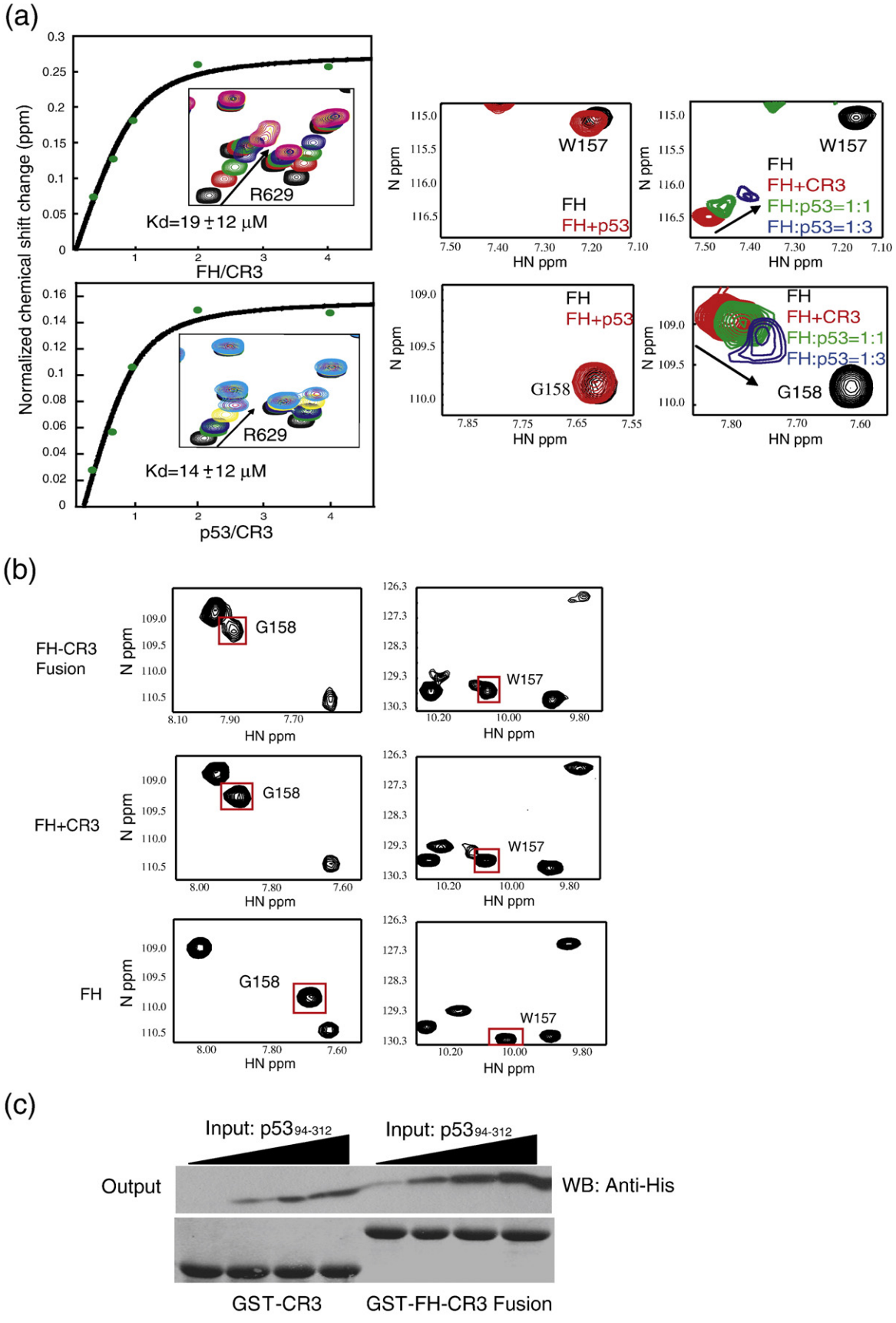

Fig. 6 (*legend on next page*)

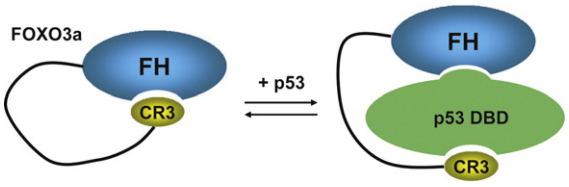

Fig. 7. Model of FOXO3a and p53 interaction. FOXO3a is in a closed state, with the CR3 domain binding to the FH domain. p53 disrupts the intramolecular interaction between the FH domain and the CR3 domain, and then both domains bind to p53. Compared with separated FH and CR3 domains, the full-length FOXO3a molecule with both parts linked together has increased binding affinity to p53.

provide large surface areas for interaction with binding partners.[29,34] Outside the highly ordered FH domain, as much as 75% of the FOXO3a molecule is predicted to be disordered. The putative disordered region resides in the long stretch between the FH domain and the CR3 domain (V252–S609), as well as in the N-terminus (M1–C150). The present biochemical and structural studies indeed confirm that the FH domain is highly ordered in nature and forms the winged-helix fold, similar to those found in this protein family.[20,21,28] In addition to specific DNA recognition by the FH domain, which mediates the well-established transcription function of FOXO3a, our results suggest that the FH domain also participates in the interaction with p53, along with the CR3 domain, at the C-terminus. Our biochemical and structural characterization of FOXO3a and p53 association revealed the unique structural characteristics of FOXO3a, involving an intramolecular interaction between the FH domain and the CR3 domain that is likely to be critical for regulating p53 interaction.

Our NMR and biochemical studies revealed that the CR3 domain plays a central role in the association with p53. The p53 DBD region binds the isolated CR3 domain with a K_d of about 14 μM, which was derived from NMR titration experiments. The FH domain also binds to p53 DBD and further augments the binding affinity between the p53 DBD and FOXO3a, as evidenced by GST pull-down assays using truncated versions of FOXO3a (Fig. 2b) as well as an engineered FH–CR3 fusion construct (Fig. 6c). Interestingly, prior to p53 binding, the CR3 domain is most likely associated with the FH domain through an intramolecular interaction with affinity ($K_d \approx 19$ μM, determined by NMR titration) similar to that for CR3 binding to p53. The binding of p53 disrupts this intramolecular interaction and promotes the association of both FH and CR3 domains with p53 (Fig. 6a). The error associated with the K_d derived from the titration of ^{15}N-labeled CR3 is relatively large, due to the small chemical shift changes, which limited the number of data points that could be collected. From the reverse NMR titration of ^{15}N-labeled FH with CR3, which exhibits larger chemical shift changes, we calculated a more accurate apparent K_d of 5 ± 1 μM for this interaction using the titration curve of the W157 peak (Supplemental Fig. 4a),[35] which is consistent with the lower limit of the value obtained in previous titration (Fig. 6a). Additionally, we found that the FH–CR3 fusion construct binds to p53 more tightly than does the CR3 domain alone (Fig. 6c), and it is likely that this intramolecular interaction between the FH domain and the CR3 domain is disrupted by p53. The affinity of the FH domain for p53 DBD was even weaker ($K_d \approx 1$ mM, estimated from GST pull-down assays). Nevertheless, the FH domain was found to be necessary for the induction of apoptosis and stabilizing p53 from degradation in functional studies.[13] It can be noted that because FH is linked to the CR3 domain, full-length FOXO may bind p53 more tightly than either domain alone as modeled by the FH–CR3 fusion protein (Fig. 6c). These results underscore the significance of the CR3 domain in the interplay between the intramolecular association with the FH domain and the interaction with p53. The CR3 domain is very rich in acidic amino acid residues and contains 5 nonpolar amino acids within the 11-residue core region (D623–M633). This core region coincides with the binding site for the FH domain, which possesses a hydrophobic cleft surrounded by positively charged residues. The CR3 peptide alone is unstructured in aqueous solution but exhibits the propensity to form an α-helix in a hydrophobic environment. Titration of the CR3 peptide with trifluoroethanol induced the formation of helical secondary structure as demonstrated by far-UV CD spectra (Supplemental Fig. 4b). Considering these results, we predict that the CR3 domain forms a helical structure when bound to the FH domain in FOXO3a or p53 DBD. Unfortunately, the severe broadening of NMR signals from the CR3 domain when bound to p53 DBD or the FH domain (data not

Fig. 6. p53 disrupts FH–CR3 interaction and binds to both domains. (a) Apparent K_d values are calculated based on the titration curves of residue R629, and $p53_{61–312}$ and the FH domain bind to the CR3 domain with similar affinity (top). The ^{1}H–^{15}N HSQC spectrum of the FH domain does not change much upon adding unlabeled $p53_{61–312}$ (left). Upon CR3 binding, peaks of W157 and G158 move from free-state positions (black) to the bound-state positions (red). With increasing $p53_{61–312}$ concentration, peaks move back toward the original free-state positions (green, FH/p53 = 1:1; blue, FH/p53 = 1:3) (right). (b) The three ^{1}H–^{15}N HSQC spectra in the left column are the signals of the backbone amide group of G158, and those in the right column are the signals of the side-chain amide group of W157. Each row represents the spectra from one protein, from top to bottom, FH–CR3 fusion, the CR3-bound FH, and the FH domain alone. (c) The p53 binding affinities for the CR3 domain and the FH–CR3 fusion protein were compared by GST pull-down assay. With the increase in input of the concentration of $p53_{94–312}$, the output $p53_{94–312}$ also increased. The output was analyzed by Western blotting, and the loading control of GST-CR3 and GST-FH–CR3 is shown at the bottom. As the molecular weights of $p53_{94–312}$ and GST-CR3 are very similar, and they ran at the same position in SDS-PAGE, the $p53_{94–312}$ ran lower in GST-CR3 lanes than in GST-FH–CR3 lanes.

shown) prevented us from determining the solution structure of the CR3 domain in these complexes.

Nuclear expulsion of p53 is thought to involve an exposure of the nuclear export signal (NES) located within the TET domain,[36] which is usually masked by the stable formation of the tetramer by the TET domain.[37] Nevertheless, the DBD of p53 is essential for p53 translocation as MDM2-dependent mono-ubiquitination of p53 in both the DBD and the TET domain promotes p53 nuclear export by exposing or activating the NES.[32,38–42] Moreover, the DBD of p53 is one of the two MDM2 binding sites,[43] and structural changes of DBD promote p53 translocation.[44] The present study revealed that it is the p53 DBD that binds to two distinct regions of FOXO3a, the FH domain and the CR3 domain, and that disrupts the intramolecular interaction between these two regions (Fig. 7). Future studies are required to illustrate the exact details of how the association of the FH and CR3 domains with p53 DBD affects p53 DBD structure and how this helps expose p53 NES, essentially resulting in translocation of p53 to the cytoplasm.

Materials and Methods

Plasmids and constructs

The FH domain (S151–A251) and the CR3 domain (D610–N650) of human FOXO3a were subcloned into pGEX-4T-1 vectors (GE Healthcare) using BamHI and XhoI restriction sites. A construct comprising the FH and CR3 domains fused by a $(Gly–Ser)_4$ linker [S151–N251–$(GS)_4$–D610–N650] was cloned into the pGEX-4T-1 vector in the same manner. The CR3 domain (D610–N650) was also subcloned into pET32a vector to produce a protein with both His and Trx tags. Three human p53 truncation constructs (M1–T312, D61–T312, and S94–T312) were subcloned into pET15b vector (Novagen) using NdeI and BamHI restriction enzyme sites. All plasmids were verified by DNA sequencing.

For *in vitro* translation, constructs of FOXO3a were amplified by PCR, digested with BamHI and XhoI, and subcloned into the corresponding sites of the expression vector pcDNA3/Myc to produce Myc-tagged fusion protein.[45] DNA fragments encoding from S151 to P491 and from S151 to P397 were amplified by PCR, and the products were digested with BamHI and BstXI to produce FOXO mutants with internal deletions. pcDNA3/MycFOXO3a$_{151–650}$ was also digested with BamHI and BstXI, and the digested PCR products were ligated. The resultant plasmids were verified by sequencing.

Overexpression and purification

The plasmids of the FH domain, the CR3 domain, the FH–CR3 fusion protein, and three p53 truncations were transformed into *Escherichia coli* BL21(DE3) cells. The cells were grown in LB medium with 100 μg/ml of ampicillin at 37 °C until an OD_{600} of 0.8 was reached and were then induced with isopropyl-β-D-thiogalactoside (IPTG) overnight at 15 °C. IPTG at 0.35 mM and that at 0.15 mM were used for FOXO proteins and p53 proteins, respectively. For labeled proteins, cultures were grown in minimal M9 medium supplemented with 100 μg/ml of ampicillin, 2 mg/l of D-biotin, 2 mg/l of thiamine–HCL, and 1 g/l of $^{15}NH_4Cl$ and 5 g/l of glucose for ^{15}N-labeled proteins and 1 g/l of $^{15}NH_4Cl$ and 2 g/l of ^{13}C-labeled glucose for doubly labeled proteins.

Cells were harvested by centrifugation and lysed by sonication. The FH domain was purified by glutathione-Sepharose 4B (GE Healthcare) and cut from the resin by thrombin at 4 °C overnight. Cleaved protein was further purified on a Hitrap SP FF (GE Healthcare) column. The CR3 domain and FH–CR3 fusion protein were both purified by glutathione-Sepharose 4B, followed by thrombin cleavage and size-exclusion chromatography on a Hiload 26/60 Superdex 75 prep grade column (GE Healthcare). The three p53 protein constructs were purified by metal affinity on Ni-nitrilotriacetic acid resin (Qiagen), eluted with 200 mM imidazole, and cut by thrombin overnight. Cleaved proteins were purified on a Hitrap SP or HP column (GE Healthcare) followed by that on a Hiload 26/60 Superdex 75 prep grade column (GE Healthcare). The purity of all proteins was confirmed by SDS-PAGE.

For expression of full-length p53, the *E. coli* strain TG1 was transformed with pGEX-p53FL plasmid, grown in LB medium to an OD_{600} of 0.4, and induced with 2 mM IPTG. After 3 h, the cells were harvested by centrifugation and lysed by sonication. The cleared lysates were mixed with 25 μl of glutathione-Sepharose beads for 1 h at 4 °C and subsequently washed five times with buffer DBN-0.1 (20 mM Hepes–KOH, pH 7.9, 0.5 mM ethylenediaminetetraacetic acid, 1 mM dithiothreitol, 20% glycerol, 100 mM KCl, and 0.1% NP-40).

A TNT Quick Coupled Transcription/Translation System (Promega) was used to express the FOXO3a deletion mutants *in vitro*. The *in vitro* translation reaction mixture was then applied to a 2-ml bed of Sephadex G-75 (GE Healthcare) in a Poly-Prep Chromatography Column (Bio-Rad) equilibrated with buffer DB-0.1. The main fraction was identified by Western blotting with a mouse monoclonal anti-Myc antibody (Cell Signaling Technology).

GST pull-down assays

Pull-down assays with *in vitro*-translated FOXO3a deletion and truncation mutants were performed by incubating precleared, *in vitro*-translated FOXO3a deletion mutants with glutathione-Sepharose-bound GST–p53 for 3 h at 4 °C. After washing the beads three times with buffer DBN-0.4 (DBN-0.1 containing 400 mM KCl) and once with buffer DBN-0.1, the proteins retained on the beads were extracted in 25 μl of SDS-PAGE sample buffer and were separated on 8%–16% Tris-Glycine Gel (Invitrogen). Proteins were detected by Western blotting with a mouse monoclonal anti-Myc antibody (Cell Signaling Technology). GST pull-down assays with purified, recombinant FOXO3a and p53 proteins expressed in *E. coli* were conducted using a GST Tag Protein Interaction Pull-Down Kit (Pierce) according to the manufacturer's instructions using phosphate-buffered saline plus 0.1% Triton X100 as the washing buffer. After washing, glutathione beads were analyzed by SDS-PAGE and Western blotting. The anti-penta-His (Qiagen) and ECL antimouse immunoglobulin G (Amersham) antibody were used as primary and secondary antibodies, respectively, to detect His-tagged proteins in Western blot analysis.

Electrophoretic mobility shift assay

DNA construct was prepared as HPLC-purified single-stranded oligos (Sigma Genosys). The double-stranded

DNA was obtained by the annealing method of mixing equal amounts of complementary oligos, heating the sample at 90–95 °C for 10 min, and cooling it to room temperature slowly.

A cy5-labeled double-stranded DNA construct derived from the PUMA promoter DNA (5′-GTTTGTTTACAAACAATG-3′; 5′-CATTGTTTGTAAACAAAC-3′) was incubated with purified FOXO3a FH domain in electrophoretic mobility shift assay buffer (20 mM Tris–HCl, pH 8.0, 40 mM KCl, 5% glycerol, 0.4 mM DTT, 0.2 mM ethylenediaminetetraacetic acid, 2 mM $MgCl_2$, 1 mg/ml of bovine serum albumin, and 1 ng/μl of poly dI/dC) for 15 min on ice. These samples were electrophoresed on 8% polyacrylamide gel at 100 V for 2.5 h at 4 °C, and the gel was visualized by a "Typhoon 9400" scanner (GE Healthcare).

NMR spectroscopy

Two-dimensional ^{1}H–^{15}N HSQC[46] spectra and three-dimensional triple-resonance HNCACB,[47] CBCACONNH,[48] and HNCO[49] spectra were collected for the backbone chemical shift assignments. The three-dimensional HCC–total COSY (TOCSY)–NNH,[50] CCCTOCSY–NNH,[51] and HCCH–TOCSY[52] spectra were collected to assign chemical shifts of side-chain atoms. ^{15}N- and ^{13}C-edited NOESY–HSQC spectra were recorded to confirm the assignments and for structure calculation. The spectra were processed and visualized by NMRPipe[53] and NMRView,[54] and resonance assignments were made using XEASY.[55] All NMR data were recorded at 25 °C on 500- or 600-MHz Varian Unity Plus spectrometers equipped with 5-mm triple-resonance cold probes and *z*-axis pulse-field gradients and an 800-MHz Bruker AVANCE II spectrometer with TCI cryoprobe. All NMR samples were prepared in a buffer containing 20 mM NaPi, pH 6.5, 50 mM KCl, 2 mM DTT, 10% or 100% D_2O, and 0.5 mM NaN_3.

NMR structure calculation

The three-dimensional structure of the FH domain was calculated by CYANA[56] using standard protocols. NOE-based restraints were obtained from CYANA-based automatic NOE assignment.[57] Estimations for φ/ψ torsion angle restraints were derived from C^{α}, C^{β}, N, and C(O) chemical shifts using TALOS.[58] Hydrogen-bond constraints were generated for protected NH groups using H_2O/D_2O solvent exchange experiments. Further water refinement was done using Crystallography & NMR System and RECOORD scripts.[59] The structure figures were prepared using PyMOL.[60]

CD spectroscopy

Far-UV CD spectra were recorded at 20 °C on a Jasco J-810 CD spectrometer at a scan rate of 20 nm/min. Data were collected in 1-nm increments from 195 to 250 nm, using a 0.1-cm path-length cell and 8 s of averaging time. The concentration of the CR3 domain sample was 0.05 mM, and it was titrated with 2, 2, 2-trifluoroethanol from 0% to 25% in 5% increments. The spectra were corrected by subtracting the spectrum of buffer.

Accession codes

The BioMagResBank accession number is 15939, and the PDB code is 2k86.

Acknowledgements

M.I. holds a Canada Research Chair in Cancer Structural Biology and C.B.M. holds a Canadian Institutes of Health Research postdoctoral fellowship. This work was supported by the Canadian Institutes of Health Research (grant awarded to M.I.). We thank Dr. Peter Stathopulos for helpful discussion and Emma Gooding for critical reading of the manuscript. We also thank the Canadian Foundation of Innovation for an 800-MHz NMR spectrometer at the Toronto Medical Discovery Tower.

Supplementary Data

Supplementary data associated with this article can be found, in the online version, at doi:10.1016/j.jmb.2008.09.025

Reference

1. Greer, E. L. & Brunet, A. (2005). FOXO transcription factors at the interface between longevity and tumor suppression. *Oncogene*, **24**, 7410–7425.
2. Kaestner, K. H., Knochel, W. & Martinez, D. E. (2000). Unified nomenclature for the winged helix/forkhead transcription factors. *Genes Dev.* **14**, 142–146.
3. Arden, K. C. & Biggs, W. H., 3rd. (2002). Regulation of the FoxO family of transcription factors by phosphatidylinositol-3 kinase-activated signaling. *Arch. Biochem. Biophys*, **403**, 292–298.
4. Anderson, M. J., Viars, C. S., Czekay, S., Cavenee, W. K. & Arden, K. C. (1998). Cloning and characterization of three human forkhead genes that comprise an FKHR-like gene subfamily. *Genomics*, **47**, 187–199.
5. Accili, D. & Arden, K. C. (2006). FoxOs at the crossroads of cellular metabolism, differentiation, and transformation. *Cell*, **117**, 421–426.
6. Barthel, A., Schmoll, D. & Unterman, T. G. (2005). FoxO proteins in insulin action and metabolism. *Trends Endocrinol. Metab.* **16**, 183–189.
7. Birkenkamp, K. U. & Coffer, P. J. (2003). Regulation of cell survival and proliferation by the FOXO (Forkhead box, class O) subfamily of Forkhead transcription factors. *Biochem. Soc. Trans.* **31**, 292–297.
8. Lynch, R. L., Konicek, B. W., McNulty, A. M., Hanna, K. R., Lewis, J. E., Neubauer, B. L. & Graff, J. R. (2005). The progression of LNCaP human prostate cancer cells to androgen independence involves decreased FOXO3a expression and reduced p27KIP1 promoter transactivation. *Mol. Cancer Res.* **3**, 163–169.
9. Tran, H., Brunet, A., Grenier, J. M., Datta, S. R., Fornace, A. J., Jr, DiStefano, P. S. *et al.* (2002). DNA repair pathway stimulated by the forkhead transcription factor FOXO3a through the Gadd45 protein. *Science*, **296**, 530–534.
10. Yang, L., Xie, S., Jamaluddin, M. S., Altuwaijri, S., Ni, J., Kim, E. *et al.* (2005). Induction of androgen receptor expression by phosphatidylinositol 3-kinase/Akt downstream substrate, FOXO3a, and their roles in apoptosis of LNCaP prostate cancer cells. *J. Biol. Chem.* **280**, 33558–33565.
11. You, H., Pellegrini, M., Tsuchihara, K., Yamamoto, K., Hacker, G., Erlacher, M. *et al.* (2006). FOXO3a-

dependent regulation of Puma in response to cytokine/growth factor withdrawal. *J. Exp. Med.* **203**, 1657–1663.
12. Nemoto, S., Fergusson, M. M. & Finkel, T. (2005). Nutrient availability regulates SIRT1 through a forkhead-dependent pathway. *Science*, **306**, 2105–2108.
13. You, H., Yamamoto, K. & Mak, T. W. (2006). Regulation of transactivation-independent proapoptotic activity of p53 by FOXO3a. *Proc. Natl Acad. Sci. USA*, **103**, 9051–9056.
14. Mihara, M., Erster, S., Zaika, A., Petrenko, O., Chittenden, T., Pancoska, P. & Moll, U. M. (2003). p53 has a direct apoptogenic role at the mitochondria. *Mol. Cell*, **11**, 577–590.
15. Wang, X. (2001). The expanding role of mitochondria in apoptosis. *Genes Dev.* **15**, 2922–2933.
16. Chipuk, J. E., Kuwana, T., Bouchier-Hayes, L., Droin, N. M., Newmeyer, D. D., Schuler, M. & Green, D. R. (2004). Direct activation of Bax by p53 mediates mitochondrial membrane permeabilization and apoptosis. *Science*, **303**, 1010–1014.
17. Chipuk, J. E., Bouchier-Hayes, L., Kuwana, T., Newmeyer, D. D. & Green, D. R. (2005). PUMA couples the nuclear and cytoplasmic proapoptotic function of p53. *Science*, **309**, 1732–1735.
18. Zou, H., Li, Y., Liu, X. & Wang, X. (1999). An APAF-1. cytochrome *c* multimeric complex is a functional apoptosome that activates procaspase-9. *J. Biol. Chem.* **274**, 11549–11556.
19. Slee, E. A., Harte, M. T., Kluck, R. M., Wolf, B. B., Casiano, C. A., Newmeyer, D. D. *et al.* (1999). Ordering the cytochrome *c*-initiated caspase cascade: hierarchical activation of caspases-2, -3, -6, -7, -8, and -10 in a caspase-9-dependent manner. *J. Cell Biol.* **144**, 281–292.
20. Clark, K. L., Halay, E. D., Lai, E. & Burley, S. K. (1993). Co-crystal structure of the HNF-3/fork head DNA-recognition motif resembles histone H5. *Nature*, **364**, 412–420.
21. Tsai, K. L., Sun, Y. J., Huang, C. Y., Yang, J. Y., Hung, M. C. & Hsiao, C. D. (2007). Crystal structure of the human FOXO3a-DBD/DNA complex suggests the effects of post-translational modification. *Nucleic Acids Res.* **35**, 6984–6994.
22. Boura, E., Silhan, J., Herman, P., Vecer, J., Sulc, M., Teisinger, J. *et al.* (2007). Both the N-terminal loop and wing W2 of the forkhead domain of transcription factor Foxo4 are important for DNA binding. *J. Biol. Chem.* **282**, 8265–8275.
23. So, C. W. & Cleary, A. L. (2002). MLL-AFX requires the transcriptional effector domains of AFX to transform myeloid progenitors and transdominantly interfere with forkhead protein function. *Mol. Cell. Biol.* **22**, 6542–6552.
24. So, C. W. & Cleary, M. L. (2003). Common mechanism for oncogenic activation of MLL by forkhead family proteins. *Blood*, **101**, 633–639.
25. Chène, P. (2001). The role of tetramerization in p53 function. *Oncogene*, **20**, 2611–2617. Review.
26. Grzesiek, S. & Bax, A. (1993). Amino acid type determination in the sequential assignment procedure of uniformly $^{13}C/^{15}N$-enriched proteins. *J. Biomol. NMR*, **3**, 185–204.
27. Wishart, D. S., Sykes, B. D. & Richards, F. M. (1991). Relationship between nuclear magnetic resonance chemical shift and protein secondary structure. *J. Mol. Biol.* **222**, 311–333.
28. Weigelt, J., Climent, I., Dahlman-Wright, K. & Wikström, M. (2001). Solution structure of the DNA binding domain of the human forkhead transcription factor AFX (FOXO4). *Biochemistry*, **40**, 5861–5869.
29. Dyson, H. J. & Wright, P. E. (2005). Intrinsically unstructured proteins and their functions. *Nat. Rev. Mol. Cell Biol.* **6**, 197–208. Review.
30. Bryson, K., McGuffin, L. J., Marsden, R. L., Ward, J. J., Sodhi, J. S. & Jones, D. T. (2005). Protein structure prediction servers at University College London. *Nucleic Acids Res.* **33**, W36–W38. Web server issue.
31. Hofseth, L. J., Hussain, S. P. & Harris, C. C. (2004). p53: 25 years after its discovery. *Trends Pharmacol. Sci.* **25**, 177–181. Review.
32. Joerger, A. C. & Fersht, A. R. (2007). Structure–function–rescue: the diverse nature of common p53 cancer mutants. *Oncogene*, **26**, 2226–2242. Review.
33. Cully, M., You, H., Levine, A. J. & Mak, T. W. (2006). Beyond PTEN mutations: the PI3K pathway as an integrator of multiple inputs during tumorigenesis. *Nat. Rev. Cancer*, **6**, 184–192. Review.
34. Sugase, K., Dyson, H. J. & Wright, P. E. (2007). Mechanism of coupled folding and binding of an intrinsically disordered protein. *Nature*, **447**, 1021–1025.
35. Cavanagh, J., Fairbrother, W. J., Palmer, A. G., 3rd, Rance, M. & Skelton, N. (2007). Protein NMR Spectroscopy: Principles and Practice, 2nd edit. Elsevier Academic Press, Burlington, MA.
36. Stommel, J. M., Marchenko, N. D., Jimenez, G. S., Moll, U. M., Hope, T. J. & Wahl, G. M. (1999). A leucine-rich nuclear export signal in the p53 tetramerization domain: regulation of subcellular localization and p53 activity by NES masking. *EMBO J.* **18**, 1660–1672.
37. Tidow, H., Melero, R., Mylonas, E., Freund, S. M., Grossmann, J. G., Carazo, J. M. *et al.* (2007). Quaternary structures of tumor suppressor p53 and a specific p53 DNA complex. *Proc. Natl Acad. Sci. USA*, **104**, 12324–12329.
38. Gu, J., Nie, L., Wiederschain, D. & Yuan, Z. M. (2001). Identification of p53 sequence elements that are required for MDM2-mediated nuclear export. *Mol. Cell. Biol.* **21**, 8533–8546.
39. Lohrum, M. A., Woods, D. B., Ludwig, R. L., Bálint, E. & Vousden, K. H. (2001). C-terminal ubiquitination of p53 contributes to nuclear export. *Mol. Cell. Biol.* **21**, 8521–8532.
40. Li, M., Brooks, C. L., Wu-Baer, F., Chen, D., Baer, R. & Gu, W. (2003). Mono- versus polyubiquitination: differential control of p53 fate by Mdm2. *Science*, **302**, 1972–1975.
41. Carter, S., Bischof, O., Dejean, A. & Vousden, K. H. (2007). C-terminal modifications regulate MDM2 dissociation and nuclear export of p53. *Nat. Cell Biol.* **9**, 428–435.
42. Nie, L., Sasaki, M. & Maki, C. G. (2007). Regulation of p53 nuclear export through sequential changes in conformation and ubiquitination. *J. Biol. Chem.* **282**, 14616–14625.
43. Shimizu, H., Burch, L. R., Smith, A. J., Dornan, D., Wallace, M., Ball, K. L. & Hupp, T. R. (2002). The conformationally flexible S9–S10 linker region in the core domain of p53 contains a novel MDM2 binding site whose mutation increases ubiquitination of p53 *in vivo*. *J. Biol. Chem.* **277**, 28446–28458.
44. Wallace, M., Worrall, E., Pettersson, S., Hupp, T. R. & Ball, K. L. (2006). Dual-site regulation of MDM2 E3-ubiquitin ligase activity. *Mol. Cell*, **23**, 251–263.
45. Obata, Y., Yamamoto, K., Miyazaki, M., Shimotohno, K., Kohno, S. & Matsuyama, T. (2005). Role of cyclophilin B in activation of interferon regulatory factor-3. *J. Biol. Chem.* **280**, 18355–18360.
46. Bodenhausen, G. & Ruben, D. (1980). Natural abundance ^{15}N NMR by enhanced heteronuclear spectroscopy. *Chem. Phys. Lett.* **69**, 185–189.

47. Wang, A. C., Lodi, P. J., Qin, J., Vuister, G. W., Gronenborn, A. M. & Clore, G. M. (1994). An efficient triple-resonance experiment for proton-directed sequential backbone assignment of medium-sized proteins. *J. Magn. Reson., Ser. B*, **105**, 196–198.
48. Grzesiek, S. & Bax, A. (1993). Amino acid type determination in the sequential assignment procedure of uniformly $^{13}C/^{15}N$-enriched proteins. *J. Biomol. NMR*, **3**, 185–204.
49. Ikura, M., Kay, L. E. & Bax, A. (1990). A novel-approach for sequential assignment of ^{1}H, ^{13}C, and ^{15}N spectra of larger proteins. Heteronuclear triple-resonance 3-dimensional NMR-spectroscopy: application to calmodulin. *Biochemistry*, **29**, 4659–4667.
50. Kay, L. E. (1997). NMR methods for the study of protein structure and dynamics. *Biochem. Cell Biol.* **75**, 1–15.
51. Grzesiek, S., Anglister, J. & Bax, A. (1993). Correlation of backbone amide and aliphatic side-chain resonances in $^{13}C/^{15}N$-enriched proteins by isotropic mixing of ^{13}C magnetization. *J. Magn. Reson., Ser. B*, **101**, 114–119.
52. Bax, A., Clore, G. M. & Gronenborn, A. M. (1990). ^{1}H–^{1}H correlation via isotropic mixing of ^{13}C magnetization, a new three-dimensional approach for assigning ^{1}H and ^{13}C spectra of ^{13}C-enriched proteins. *J. Magn. Reson.* **88**, 425–431.
53. Delaglio, F., Grzesiek, S., Vuister, G. W., Zhu, G., Pfeifer, J. & Bax, A. (1995). NMRPipe: a multidimensional spectral processing system based on UNIX pipes. *J. Biomol. NMR*, **6**, 277–293.
54. Johnson, B. A. (2004). Using NMRView to visualize and analyze the NMR spectra of macromolecules. *Methods Mol. Biol.* **278**, 313–352.
55. Bartels, C., Xia, T., Billeter, M., Guntert, P. & Wuthrich, K. (1995). The program XEASY for computer-supported NMR spectral analysis of biological macromolecules. *J. Biomol. NMR*, **6**, 1–10.
56. Güntert, P., Mumenthaler, C. & Wüthrich, K. (1998). Torsion angle dynamics for NMR structure calculation with the new program DYANA. *J. Mol. Biol.* **273**, 283–298.
57. Herrmann, T., Guntert, P. & Wuthrich, K. (2002). Protein NMR structure determination with automated NOE assignment using the new software CANDID and the torsion angle dynamics algorithm DYANA. *J. Mol. Biol.* **319**, 209–227.
58. Cornilescu, G., Delaglio, F. & Bax, A. (1999). Protein backbone angle restraints from searching a database for chemical shift and sequence homology. *J. Biomol. NMR*, **13**, 289–302.
59. Nederveen, A. J., Doreleijers, J. F., Vranken, W., Miller, Z., Spronk, C. A., Nabuurs, S. B. *et al.* (2005). RECOORD: a recalculated coordinate database of 500+ proteins from the PDB using restraints from the BioMagResBank. *Proteins*, **59**, 662–672.
60. DeLano, W. L. (2002). The PyMOL Molecular Graphics System. DeLano Scientific, Palo Alto, CA. http://www.pymol.org.